



THE UNIVERSITY *of* EDINBURGH

Edinburgh Research Explorer

Differential Ly-6C expression identifies the recruited macrophage phenotype, which orchestrates the regression of murine liver fibrosis

Citation for published version:

Ramachandran, P, Pellicoro, A, Vernon, MA, Boulter, L, Aucott, RL, Ali, A, Hartland, SN, Snowdon, VK, Cappon, A, Gordon-Walker, TT, Williams, MJ, Dunbar, DR, Manning, J, van Rooijen, N, Fallowfield, JA, Forbes, SJ & Iredale, JP 2012, 'Differential Ly-6C expression identifies the recruited macrophage phenotype, which orchestrates the regression of murine liver fibrosis' Proceedings of the National Academy of Sciences, vol 109, no. 46, pp. E3186-E3195. DOI: 10.1073/pnas.1119964109

Digital Object Identifier (DOI):

[10.1073/pnas.1119964109](https://doi.org/10.1073/pnas.1119964109)

Link:

[Link to publication record in Edinburgh Research Explorer](#)

Document Version:

Publisher's PDF, also known as Version of record

Published In:

Proceedings of the National Academy of Sciences

Publisher Rights Statement:

Freely available online through the PNAS open access option.

General rights

Copyright for the publications made accessible via the Edinburgh Research Explorer is retained by the author(s) and / or other copyright owners and it is a condition of accessing these publications that users recognise and abide by the legal requirements associated with these rights.

Take down policy

The University of Edinburgh has made every reasonable effort to ensure that Edinburgh Research Explorer content complies with UK legislation. If you believe that the public display of this file breaches copyright please contact openaccess@ed.ac.uk providing details, and we will remove access to the work immediately and investigate your claim.



Differential Ly-6C expression identifies the recruited macrophage phenotype, which orchestrates the regression of murine liver fibrosis

Prakash Ramachandran^a, Antonella Pellicoro^a, Madeleine A. Vernon^a, Luke Boulter^a, Rebecca L. Aucott^a, Aysha Ali^a, Stephen N. Hartland^a, Victoria K. Snowdon^a, Andrea Cappon^{a,b}, Timothy T. Gordon-Walker^a, Mike J. Williams^a, Donald R. Dunbar^c, Jonathan R. Manning^c, Nico van Rooijen^d, Jonathan A. Fallowfield^a, Stuart J. Forbes^a, and John P. Iredale^{a,1}

^aUniversity of Edinburgh/Medical Research Council Centre for Inflammation Research and ^cUniversity of Edinburgh Bioinformatics Core, Centre for Cardiovascular Sciences, The Queen's Medical Research Institute, Edinburgh EH16 4TJ, United Kingdom; ^bDepartment of Surgical, Oncological and Gastroenterological Sciences, Padova University Hospital, 35128 Padova, Italy; and ^dDepartment of Molecular Cell Biology, Vrije Universiteit, 1081 BT, Amsterdam, The Netherlands

Edited by Mina J Bissell, E. O. Lawrence Berkeley National Laboratory, Berkeley, CA, and approved September 24, 2012 (received for review December 29, 2011)

Although macrophages are widely recognized to have a profibrotic role in inflammation, we have used a highly tractable CCl₄-induced model of reversible hepatic fibrosis to identify and characterize the macrophage phenotype responsible for tissue remodeling: the hitherto elusive restorative macrophage. This CD11B^{hi} F4/80^{int} Ly-6C^{lo} macrophage subset was most abundant in livers during maximal fibrosis resolution and represented the principle matrix metalloproteinase (MMP) -expressing subset. Depletion of this population in CD11B promoter–diphtheria toxin receptor (CD11B-DTR) transgenic mice caused a failure of scar remodeling. Adoptive transfer and *in situ* labeling experiments showed that these restorative macrophages derive from recruited Ly-6C^{hi} monocytes, a common origin with profibrotic Ly-6C^{hi} macrophages, indicative of a phenotypic switch *in vivo* conferring proresolution properties. Microarray profiling of the Ly-6C^{lo} subset, compared with Ly-6C^{hi} macrophages, showed a phenotype outside the M1/M2 classification, with increased expression of MMPs, growth factors, and phagocytosis-related genes, including *Mmp9*, *Mmp12*, insulin-like growth factor 1 (*Igf1*), and Glycoprotein (transmembrane) *nmb* (*Gpnb*). Confocal microscopy confirmed the postphagocytic nature of restorative macrophages. Furthermore, the restorative macrophage phenotype was recapitulated *in vitro* by the phagocytosis of cellular debris with associated activation of the ERK signaling cascade. Critically, induced phagocytic behavior *in vivo*, through administration of liposomes, increased restorative macrophage number and accelerated fibrosis resolution, offering a therapeutic strategy to this orphan pathological process.

Kupffer Cell | collagen | degradation | myofibroblast | proliferation

As the generic and common pathological endpoint to chronic injury, fibrosis has been estimated to contribute to 45% of all deaths in industrialized nations (1, 2). Currently, no direct antifibrotic therapeutic interventions exist. Long thought of as inexorably progressive, recent evidence, particularly in the liver (3) but also the kidney (4), lung (5, 6), and heart (7), indicates that some reversibility exists, even in advanced disease. Therefore, a more detailed understanding of the specific mechanisms governing fibrosis regression will likely inform therapeutic approaches.

Macrophages have long been implicated in promoting tissue fibrosis (8–10). However, it has recently been shown that they also play a pivotal role in fibrosis regression (6, 11), in part through expression of matrix-degrading metalloproteinase enzymes (MMPs) (12). Macrophages are capable of distinct activation states and functions, which *in vitro*, can be broadly classified as M1 (classical) or M2 (alternative) (13, 14). It is generally postulated that M1 macrophages are proinflammatory, whereas M2 macrophages are

responsible for immunomodulation and wound-healing responses (14). However, it is increasingly clear that this binary classification does not address the more complex heterogeneity *in vivo*, where macrophages adopt distinct phenotypes and even switch between phenotypes in response to the myriad of stimuli to which they are exposed (13). These *in vivo* macrophage phenotypes are impossible to recapitulate exactly in tissue culture models, emphasizing the importance of the characterization of macrophages on the basis of function (13).

Ly-6C is a cell surface glycoprotein that is widely used to identify functionally discrete murine circulating monocyte populations: Ly-6C^{hi} monocytes (analogous to CD14^{hi} CD16^{lo} human monocytes) are recruited early to inflammatory environments and thought to be proinflammatory, whereas Ly-6C^{lo} monocytes (analogous to CD14^{lo} CD16^{hi} human monocytes) are a more patrolling cell type and can replenish resident tissue macrophages (15, 16). Differential Ly-6C expression in diseased tissues has identified functionally distinct macrophage populations (17–20). Indeed, an Ly-6C^{hi} intrahepatic macrophage population, derived from recruitment of circulating Ly-6C^{hi} monocytes, is critical for fibrogenesis (21). However, the nature, origin, and phenotype of the macrophage subset responsible for mediating fibrosis resolution have not been defined.

In this study, we have exploited differential Ly-6C expression in a tractable and reproducible model of reversible murine hepatic fibrosis to identify the specific macrophage population responsible for fibrosis resolution: the restorative macrophage. We have gone on to characterize this cell, and we have shown categorically that it is derived from recruited inflammatory monocytes after a phenotypic switch mediated by the ingestion of cellular debris and that it represents a newly identified phenotype distinct from the M1/M2 paradigm. Finally, we have established this mechanism to manipulate macrophage phenotype *in vivo* and accelerate fibrosis resolution.

Author contributions: P.R., A.P., M.A.V., L.B., S.N.H., S.J.F., and J.P.I. designed research; P.R., A.P., M.A.V., L.B., R.L.A., A.A., S.N.H., V.K.S., A.C., T.T.G.-W., and M.J.W. performed research; N.v.R. contributed new reagents/analytic tools; P.R., A.P., D.R.D., and J.R.M. analyzed data; and P.R., J.A.F., S.J.F., and J.P.I. wrote the paper.

The authors declare no conflict of interest.

This article is a PNAS Direct Submission.

Freely available online through the PNAS open access option.

Data deposition: The microarray data reported in the paper have been deposited in the ArrayExpress database, www.ebi.ac.uk/arrayexpress (accession no. E-MEXP-3177).

¹To whom correspondence should be addressed. E-mail: john.iredale@ed.ac.uk.

See Author Summary on page 18649 (volume 109, number 46).

This article contains supporting information online at www.pnas.org/lookup/suppl/doi:10.1073/pnas.1119964109/-DCSupplemental.

Results

Experimental Liver Fibrosis Shows Distinct Phases of Fibrogenesis and Resolution.

We established a model of liver fibrosis reversal from which macrophage populations could be isolated on a day-to-day basis. C57BL/6 mice were administered two times weekly i.p. carbon tetrachloride (CCl₄) for 4 wk followed by tissue harvests 24, 48, 72, 96, 168, and 256 h after the final CCl₄ injection (Fig. 1A). Comparison was made with age-matched uninjured (control) animals. Hepatic fibrosis and myofibroblast activation were assessed by immunohistochemistry and morphometric analysis of picrosirius red (PSR), collagen 1, collagen 3, and α -smooth muscle actin (α -SMA). Liver fibrosis and myofibroblast activation (α -SMA) peaked at 48–72 h, identifying 24 h as a time of active fibrogenesis, whereas maximal scar resolution and reduction in myofibroblast area occurred between 72 and 96 h and was followed by a more protracted regression of the residual fibrosis (96–256 h) (Fig. 1B and C). Scar resolution occurred after reduction in overall hepatic damage as assessed by serum alanine aminotransferase (ALT) and aspartate aminotransferase (AST) levels (Fig. 1D). Additionally, at the initiation of scar resolution, there was a significant reduction in hepatic levels of Il-1 β , Ccl2, Ccl3, and Cxcl2, suggesting an overall change in macrophage phenotype (Fig. 1E). As we have previously shown (3), loss of liver Timp-1 at a gene and protein level preceded fibrosis regression (Fig. S1A and B).

Ly-6C^{lo} Monocyte-Derived Macrophages Predominate During Maximal Fibrosis Resolution and Represent the Principle MMP-Expressing Subset.

Having identified the time of early and maximal fibrosis resolution (72 h), we determined whether there were associated changes in specific hepatic macrophage subsets. Total hepatic macrophages were identified on flow cytometry as viable CD45⁺ Ly-6G[–] NK1.1[–] CD3[–] B220[–] CD11B⁺ F4/80⁺ cells from the nonparenchymal cell fraction of digested livers (Fig. S2A–E). Importantly, coinciding with maximal fibrosis resolution, total hepatic macrophage number peaked at 72 h (Fig. 2A), and macrophages closely associated with hepatic scars topographically (Fig. 2B).

Flow cytometric analysis of hepatic macrophages enabled identification of distinct subsets. F4/80^{hi} CD11B^{intermediate} macrophages predominated in the control (uninjured) liver and represent the resident Kupffer cell population (22) (Fig. 2C). The proportion of resident macrophages was reduced during active inflammation/fibrogenesis (24 h) and progressively increased during resolution (Fig. 2C and E). The CD11B^{hi} F4/80^{intermediate} subset represents a recruited monocyte-derived macrophage population (22). Analysis of Ly-6C expression on this subset identified two clearly distinct hepatic recruited macrophage populations: Ly-6C^{hi} and Ly-6C^{lo} (Fig. 2D). Dynamic changes in these macrophage populations were seen during fibrogenesis and resolution (Fig. 2D and E). Whereas during fibrogenesis (24 h), Ly-6C^{hi} (profibrotic) macrophages were the predominant subset (21) (Fig. 2E), at maximal scar resolution (72 h), when macrophage number peaked, there was a reduction in the Ly-6C^{hi} population and a dramatic and significant increase in Ly-6C^{lo} macrophages, which became the dominant population (Fig. 2E). Overall, these changes were also evident when absolute macrophage numbers were quantified (Fig. 2F). Therefore, Ly-6C^{lo} monocyte-derived macrophages at the time of maximal scar resolution represented the most numerous macrophage population seen throughout the injury and recovery phases (4.13 \pm 0.5-fold more than the total number of macrophages in the undamaged liver).

During late resolution (168 h), the relative proportions of macrophage subsets returned to control liver, although there remained an increase in the proportion of the Ly-6C^{lo} subset (Fig. 2E). We have previously shown that macrophage MMP expression is critical for fibrosis regression (12). To identify the principle hepatic MMP-expressing macrophage subset, we used a pan-MMP substrate (MMPsense), which becomes fluorescent after cleavage

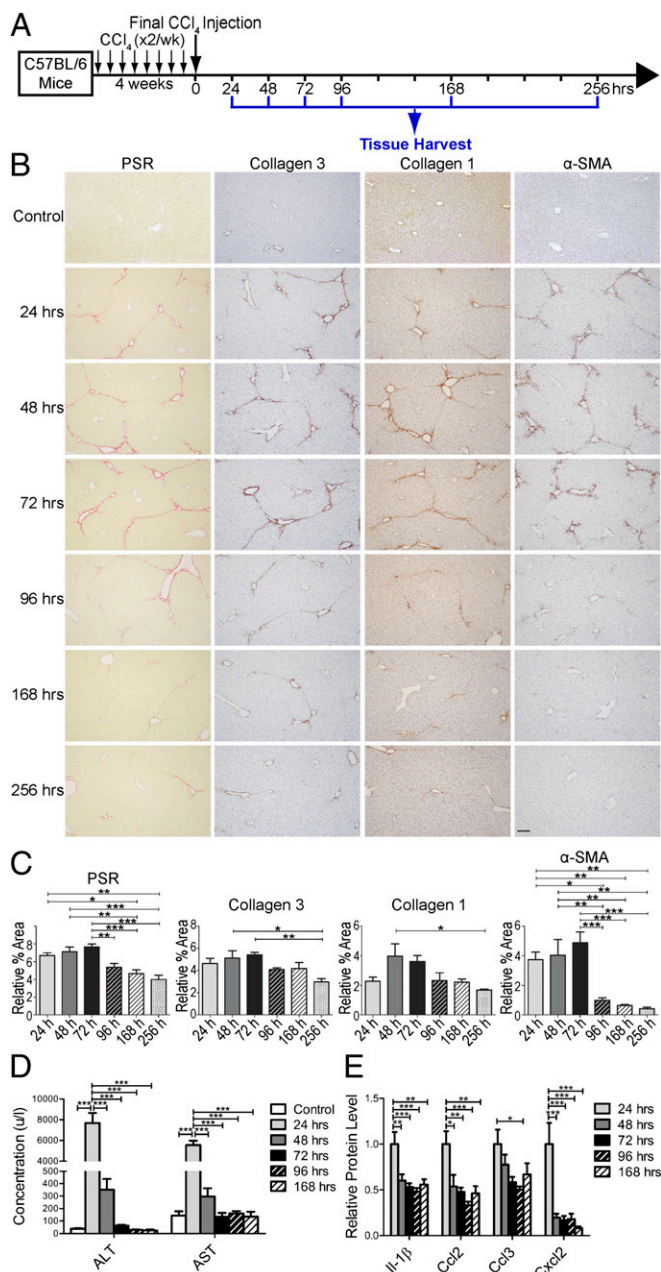


Fig. 1. Experimental liver fibrosis shows distinct phases of fibrogenesis and resolution. (A) Schematic representation of the model of reversible hepatic fibrosis in C57BL/6 mice by 4 wk of two times per week i.p. CCl₄ followed by harvest at serial time points after the final injection. Comparisons were made with control (uninjured) animals. (B and C) Histological characterization of hepatic fibrosis and myofibroblast activation by PSR, collagen 1, collagen 3, and α -SMA immunohistochemistry. (B) Representative images are shown for control animals and each time point. (Scale bar: 100 μ m.) (C) Quantification of histological changes by morphometric pixel analysis expressed relative to mean percent area of control animals ($n = 4$ per time point; representative of three independent experiments). (D) Serum ALT and AST levels in control mice and at stated time point after the final CCl₄ dose ($n = 5$ –6 per time point from two independent experiments). (E) Whole-liver protein levels of Il-1 β , Ccl2, Ccl3, and Cxcl2 measured by multiplex cytokine assay expressed relative to mean protein concentration at the 24-h time point for each ($n = 7$ –9 per time point from two independent experiments). All data shown as mean \pm SEM. * $P < 0.05$, ** $P < 0.01$, *** $P < 0.001$.

by active MMPs in vivo (23), enabling us to identify a population of MMPsense-positive hepatic macrophages by flow cytometry (Fig.

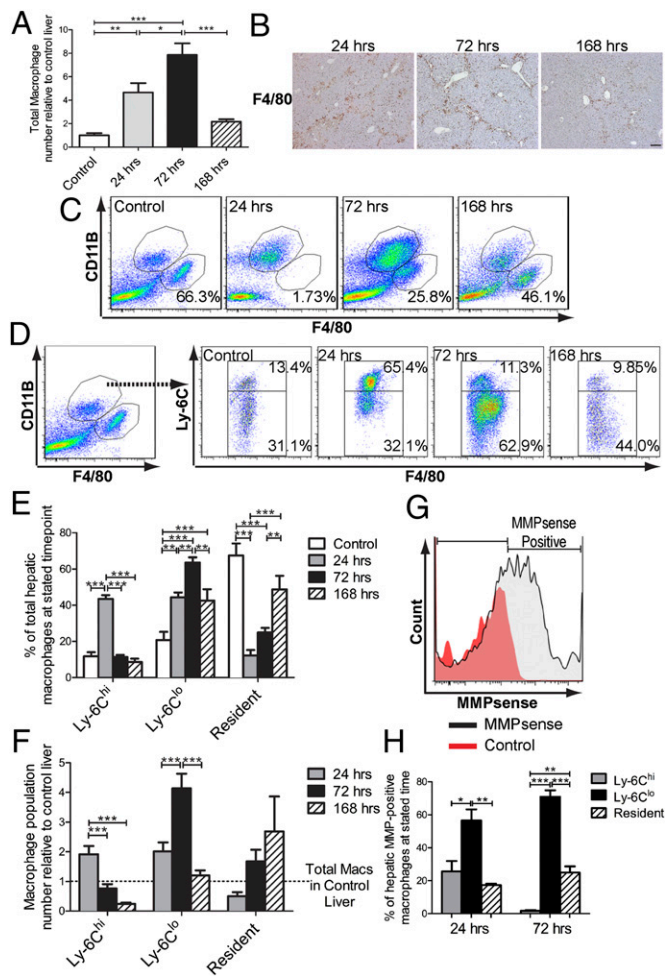


Fig. 2. Ly-6C^{lo} macrophages predominate during maximal fibrosis resolution and represent the principle MMP expressing subset. (A–G) Analysis of hepatic macrophages at 24 (inflammation/fibrogenesis), 72 (early and maximal scar resolution), and 168 h (late resolution) after the final CCl₄ injection. Comparison was made to control (uninjured) mice. (A) Total hepatic macrophage number quantified by flow cytometry expressed relative to the mean number of macrophages in control liver ($n = 8–12$ per time point from two independent experiments). (B) F4/80 immunohistochemistry indicates that macrophages localize around areas of scar at 72 h. (Scale bar: 100 μm .) (C) F4/80^{hi} CD11B^{int} resident Kupffer cells during injury and resolution (representative percentages indicate F4/80^{hi} CD11B^{int} cells as a proportion of total macrophages). (D) Subset analysis of CD11B^{hi} F4/80^{int} monocyte-derived macrophages on the basis of differential Ly-6C expression identifies two distinct populations: Ly-6C^{hi} and Ly-6C^{lo} with dynamic changes during injury and resolution (representative percentages indicate each subset as a proportion of total hepatic macrophages). (E) Quantification of Ly-6C^{hi}, Ly-6C^{lo}, and resident macrophage subsets as a proportion of total hepatic macrophage number ($n = 10–17$ per time point from four independent experiments). (F) Relative number per liver of each macrophage subset at each time point expressed relative to mean total macrophage number in control liver ($n = 12–17$ per time point from four independent experiments). (G and H) After 4 wk of CCl₄, mice were given fluorescent MMP substrate (MMPsense) or vehicle control at 0 or 48 h with harvest at 24 or 72 h, respectively. (G) Identification of MMPsense-positive macrophages at 24 and 72 h by flow cytometry. (H) Macrophage subset analysis of MMPsense-positive macrophage population at 24 and 72 h ($n = 3–4$). All data shown as mean \pm SEM. * $P < 0.05$, ** $P < 0.01$, *** $P < 0.001$. Representative flow cytometry plots, histograms, and images are shown.

2G). Subset analysis of these cells during both fibrogenesis (24 h) and maximal matrix degradation (72 h) showed that the predominant active MMP-expressing macrophage population at both

time points was the Ly-6C^{lo} macrophage (Fig. 2H). Therefore, Ly-6C^{lo} monocyte-derived macrophages accumulate maximally during the most rapid phase of fibrosis resolution. Furthermore, they represent the principle MMP-expressing population during both fibrogenesis and fibrosis regression.

Depletion of CD11B-Positive Macrophages Defines Ly-6C^{lo} Cells as Being Critical for Scar Resolution.

To define the functional role of distinct macrophage subsets in mediating scar resolution, a well-described selective in vivo macrophage depletion strategy was used (11). CD11B promoter - diphtheria toxin receptor (CD11B-DTR) transgenic mice were given CCl₄ for 4 wk. To ensure maximal macrophage depletion throughout the rapid phase of scar resolution, i.v. diphtheria toxin (DT) (or PBS control) was administered 48, 72, and 96 h after the final CCl₄ injection followed by harvest at 120 h (Fig. 3A). In concordance with previous data (17), administration of DT was effective in depleting both populations of circulating monocytes (Ly-6C^{hi} and Ly-6C^{lo}) (Fig. S3A and B). The degree of depletion was more profound for the Ly-6C^{lo} monocytes in keeping with them being a more mature cell type forming from differentiation of Ly-6C^{hi} monocytes (15) and thus, taking longer to replenish after depletion (24).

We proceeded to analyze hepatic macrophage subsets in CD11B-DTR mice (Fig. 3B and C). Importantly, administration of DT during maximal fibrosis resolution, when Ly-6C^{lo} intrahepatic macrophages predominate, induced significant depletion of this subset until harvest, causing a $76.7 \pm 3.16\%$ reduction in relative number at 120 h (Fig. 3B and C). No depletion of the smaller population of hepatic Ly-6C^{hi} macrophages was seen, whereas there was a minor increase in the resident macrophage number (Fig. 3C). For comparison, we depleted macrophages during the inflammatory/fibrogenic phase when both Ly-6C^{hi} and Ly-6C^{lo} hepatic macrophages are present in large numbers. DT was administered to CD11B-DTR mice 8 h after final CCl₄, with harvest at 24 h. Using this strategy, we observed a more general depletion of both Ly-6C^{hi} and Ly-6C^{lo} monocyte-derived macrophage subsets (Fig. S3C). Thus, timing depletion for when an individual population predominates is critical for selectivity. What is also apparent from these data is that the Ly-6C^{lo} hepatic macrophage subset is more susceptible to depletion after DT than the Ly-6C^{hi} subset. This result is likely to reflect the higher level of CD11B expression in Ly-6C^{lo} macrophages than the Ly-6C^{hi} subset (Fig. S3D). Importantly, DT administration during fibrosis regression did not induce a change in the number of hepatic neutrophils or CD3-positive cells (Fig. S3E and F). Furthermore, this depletion strategy caused persistent fibrosis, indicating a failure to remodel the hepatic scar (Fig. 3D and E). No difference was detected in the α -SMA area after macrophage depletion, suggesting that the observed phenotype was a result of reduced matrix degradation rather than increased myofibroblast activation (Fig. 3D and E). To confirm the specificity of these findings, we administered DT (or PBS control) to WT mice according to the same schedule (Fig. 3A). DT administration to WT mice had no effect on macrophage subsets or hepatic fibrosis (Fig. S3G and H). To further show the specific effect of hepatic Ly-6C^{lo} macrophages on fibrosis regression, we identified a statistically significant inverse correlation between the number of Ly-6C^{lo} macrophages and the degree of fibrosis (Fig. 3F), indicating that the degree of depletion of this subset directly relates to the amount of residual scar. Critically, no significant correlations were seen between the number of Ly-6C^{hi} or resident macrophages and the degree of fibrosis (Fig. S3I and J).

These findings indicate that Ly-6C^{lo} macrophages are critical for the resolution of hepatic fibrosis and the restoration of normal tissue architecture. Furthermore, given the temporal and numerical association of the Ly-6C^{lo} subset with the time of maximal scar degradation (Fig. 2D–F) and the fact that they are the principle MMP-expressing population (Fig. 2H), we postulated that these represent the elusive restorative macrophages.

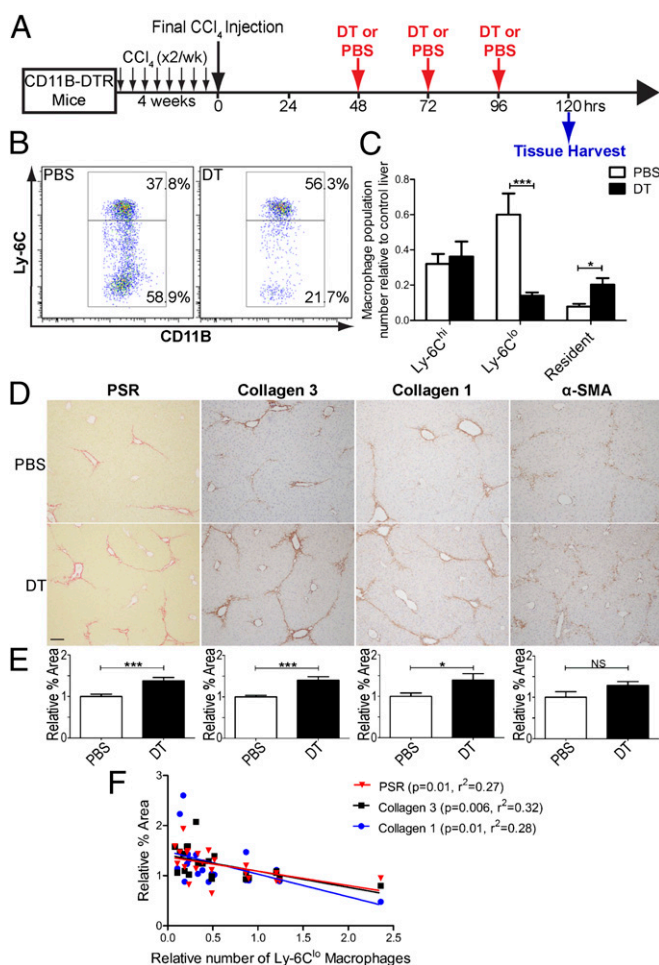


Fig. 3. Depletion of CD11B-positive macrophages defines Ly-6C^{lo} cells as being critical for scar resolution. (A) Schematic representation of model of macrophage depletion during fibrosis resolution in CD11B-DTR mice by administration of DT (or PBS control). (B) Flow cytometry data from livers of PBS and DT-treated mice gated on viable CD45+ Ly-6G- CD11B^{hi} F4/80^{int} hepatic macrophages (representative percentages of each subset as a proportion of total macrophage number shown). (C) Quantification of relative number of each macrophage subset expressed relative to mean total macrophage number in PBS-treated livers ($n = 11-13$ from two independent experiments). (D) Representative PSR staining and immunohistochemistry of collagen 1, collagen 3, and α -SMA after macrophage depletion or control. (Scale bar: 100 μ m.) (E) Quantification of histological changes by pixel analysis expressed relative to mean percent area in PBS-treated liver ($n = 10-12$ from two independent experiments). (F) Correlation of degree of fibrosis assessed by PSR, collagen 1, and collagen 3 area with the relative number of Ly-6C^{lo} macrophages ($n = 22$ from two independent experiments). All data shown as mean \pm SEM. * $P < 0.05$, *** $P < 0.001$. NS, nonsignificant. Representative flow cytometry plots and images are shown.

CD11c+ dendritic cells (DCs) have been associated with resolution of liver injury (25, 26) and share a number of cell surface markers with macrophages (27). The restorative macrophage subset at 72 h expressed only intermediate levels of CD11c (Fig. S4A). Furthermore, administration of DT to chronically injured CD11c-DOG mice at a dose known to deplete hepatic DCs (28) had no effect on the identified hepatic macrophage subsets (Fig. S4B and C), indicating no significant contribution of hepatic DCs to these populations.

Ly-6C^{lo} Macrophages Derive from an in Situ Phenotypic Switch of Recruited Ly-6C^{hi} Monocytes. The profibrotic Ly-6C^{hi} macrophage subset has been shown to derive from a Chemokine (C-C motif)

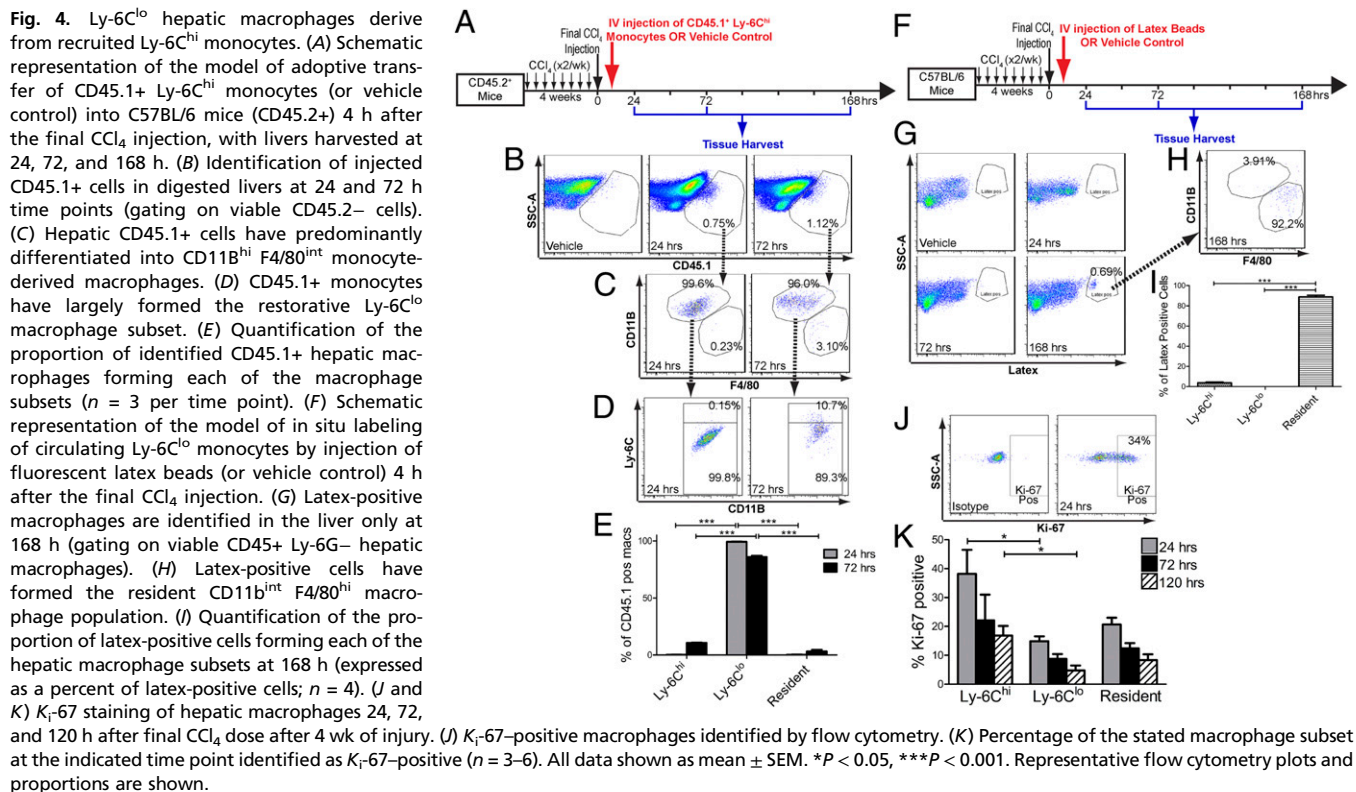
receptor 2 (CCR2)-dependent recruitment of circulating Ly-6C^{hi} monocytes (21). Given that hepatic Ly-6C^{lo} macrophages are also monocyte-derived (Fig. 2D), restorative macrophages must have an origin from recruited Ly-6C^{hi} or Ly-6C^{lo} monocytes. Blood analysis showed that, during active fibrogenesis (24 h), there was an increased number of both populations of circulating monocytes, whereas during maximal resolution (72 h), only the Ly-6C^{hi} monocytes remained elevated (Fig. S5A-C).

To determine which of the circulating monocyte populations contributed to the formation of the restorative macrophages, adoptive transfer and in vivo labeling experiments were performed. For adoptive transfer, hepatic fibrosis was induced in C57BL/6 mice (CD45.2+); 4 h after the final CCl₄ injection, we injected 9×10^5 FACS-sorted bone marrow-derived CD45.1+ Ly-6C^{hi} monocytes (Ly-6G- CD115+ CD11B+ Ly-6C^{hi} cells) (Fig. S5D) or vehicle control through the tail vein, with harvests at 24, 72, and 168 h (Fig. 4A). Adoptively transferred CD45.1+ Ly-6C^{hi} monocytes could be detected in livers during active fibrogenesis (24 h) and early resolution (72 h) but not during late resolution (Fig. 4B). Even at 24 h, these monocytes had differentiated into Ly-6C^{lo} macrophages (Fig. 4C-E). This population remained the predominant macrophage population formed from the adoptively transferred monocytes at 72 h (Fig. 4C-E). To determine the relative contribution of Ly-6C^{lo} monocytes to the hepatic macrophage subsets, we used a well-validated in vivo labeling technique (29, 30). After chronic injury with 4 wk of CCl₄, mice were given 200 μ L fluorescent latex beads (which selectively label circulating Ly-6C^{lo} monocytes) through the tail vein 4 h after the final CCl₄ injection. Animals were harvested at 24, 72, and 168 h (Fig. 4F). This technique caused selective labeling of circulating Ly-6C^{lo} monocytes (Fig. S5E and F) as previously shown (29, 30). Latex-positive cells could not be identified in livers at 24 or 72 h, despite concurrent positive circulating Ly-6C^{lo} monocytes (Fig. 4G). However, a population of intrahepatic latex-positive cells emerged during late resolution (168 h) (Fig. 4H), predominantly in the resident macrophage population (Fig. 4H and I).

Recent work has also shown a key role for local proliferation in the accumulation of macrophages during chronic inflammation (31). Given the dramatic increase in the number of Ly-6C^{lo} macrophages at maximal resolution (Fig. 2F), we determined the contribution of local macrophage proliferation to this population. Using flow cytometric Ki-67 staining on hepatic nonparenchymal cells after 4 wk of CCl₄, we could identify proliferative hepatic macrophages (Fig. 4J). Interestingly, the recruited proinflammatory Ly-6C^{hi} macrophage population represented the most proliferative macrophage subset at 24, 72, and 120 h after the final CCl₄ injection (Fig. 4K). The fact that the number of Ly-6C^{hi} macrophages rapidly declines (Fig. 2E and F) in the context of active proliferation emphasizes that this population undergoes a switch in phenotype in vivo.

These data show that restorative Ly-6C^{lo} macrophages derive from circulating Ly-6C^{hi} monocytes, a common origin to profibrotic macrophages, and that an in vivo phenotypic switch leads to fibrosis-modifying capabilities. Furthermore, Ly-6C^{lo} monocytes make no contribution to the proresolution population but contribute to repopulating the resident macrophage pool during late resolution.

Ly-6C^{lo} Macrophages Show a Characteristic Gene Expression Profile Favoring Scar Resolution. Having identified that Ly-6C^{lo} macrophages, derived from a phenotypic switch of Ly-6C^{hi} monocytes, are critical for regression of hepatic fibrosis, we sought to define the mediators produced by this newly identified macrophage subset that confer its restorative properties. Affymetrix mouse gene microarrays were performed on FACS-sorted restorative 72-h Ly-6C^{lo} macrophages and compared with the profibrotic 24-h Ly-6C^{hi} macrophages given their common origin, distinct functional roles, and relative predominance at critical time points in



the fibrogenesis resolution model. Specific microarray hits were confirmed by quantitative PCR.

A number of differentially regulated genes were identified, and the full list is available in Tables S1 and S2. In keeping with the critical role of macrophage MMP expression in fibrosis resolution (12), the switch to a proresolution macrophage phenotype was associated with an up-regulation of MMPs (Fig. 5A). Furthermore, a number of proinflammatory cytokines and chemokines were down-regulated, and concurrently, genes associated with an antiinflammatory macrophage program [e.g. Chemokine (C-X3-C) receptor 1 (CX3CR1)] (32) or antifibrotic effects (e.g. Macrophage migration inhibitory factor (MIF) and CD74) (33) were increased (Fig. 5A). Expression of TGF- β , the archetypal profibrotic cytokine, was reduced in the restorative macrophage population along with Thrombospondin-1 (Thbs1), a potent activator of latent TGF- β (34). We also identified additional proresolution mechanisms, such as a strong increase in expression of insulin-like growth factor 1 (Igf1), which has been implicated as being antifibrotic (35) (Fig. 5A). Thus, the switch to a restorative macrophage phenotype confers a number of proresolution features, highlighting the importance of a cellular mechanism for tissue fibrosis regression.

We performed pathway enrichment analysis on the differentially regulated genes from the two macrophage populations using the DAVID bioinformatics tool (36, 37). The proinflammatory macrophage population was enriched for pathways, including response to wounding, coagulation cascade, and chemotaxis (Fig. S6A), which are important for fibrogenesis (38, 39). Analysis of the restorative macrophages showed enrichment for pathways, such as lysosomes, endocytosis, scavenger receptors, and antigen presentation, which are implicated in phagocytosis (Fig. S6B). We also identified enhancement of pathways implicated in fatty acid metabolism and peroxisome proliferator activated receptor (PPAR) signaling (Fig. S6B). The enrichment of phagocytosis-related genes was confirmed individually, where a number of opsonins, receptors, and genes involved in the recognition, binding, and clearance of apoptotic cells were up-regulated in the re-

storative macrophage population (Fig. 5B). Similarly, a number of PPAR- γ target genes was up-regulated in these proresolution macrophages (Fig. 5B). We also assessed the degree of expression of a number of previously described M1 and M2 macrophage markers to determine how hepatic inflammatory and restorative macrophages fit into the traditional paradigm (Fig. 5A and B). Although Ly-6C^{lo} restorative macrophages show increased expression of some M2 genes, such as Macrophage Mannose receptor 1 (Mrc1), Arginase-1 (Arg1), and Retnla (Fizz-1), they also down-regulate other characteristic M2 genes, including Chi3l3 (YM-1), Il-1 receptor antagonist (Il1rn), Kdm6b (Jmjd3), Ccl24, Il-10, and TGF- β (14, 40). Simultaneously, these Ly-6C^{lo} macrophages up-regulate traditional M1 genes, such as Ciita (MHC class II transactivator), CD16, CD32, and Serpine1 (plasminogen activator inhibitor type 1) (14, 40, 41). Therefore, these hepatic macrophage populations do not fit into the M1/M2 classification and represent newly identified macrophage phenotypes (Fig. 5B).

We proceeded to confirm a number of the gene expression changes at a protein level using flow cytometry (Fig. 5C). Additionally, by administering MMPsense 24 h before harvest, we showed that the switch from inflammatory to restorative macrophage phenotype resulted in an increase in active MMP expression (Fig. 5C). Our microarray data also enabled us to identify the functionally distinct macrophage subsets in situ using immunohistochemistry for Chi3l3, MMP-12, and Glycoprotein (transmembrane) nmb (Gpnm) (Fig. 5D). We confirmed the specificity of these markers in our CD11B-DTR depletion model, where the administration of DT causes a significant reduction in the number of MMP-12-positive cells histologically (Fig. S6C), whereas there was no significant difference in the number of Chi3l3-positive cells (Fig. S6D), mirroring the changes seen on flow cytometry (Fig. 3B and C). We went on to show the presence of similar MMP-12- and GPNMB-expressing cells associated with scars in cirrhotic human livers (Fig. 5D) and have identified them as a subpopulation of human CD68-positive macrophages (Fig. S6E and F).

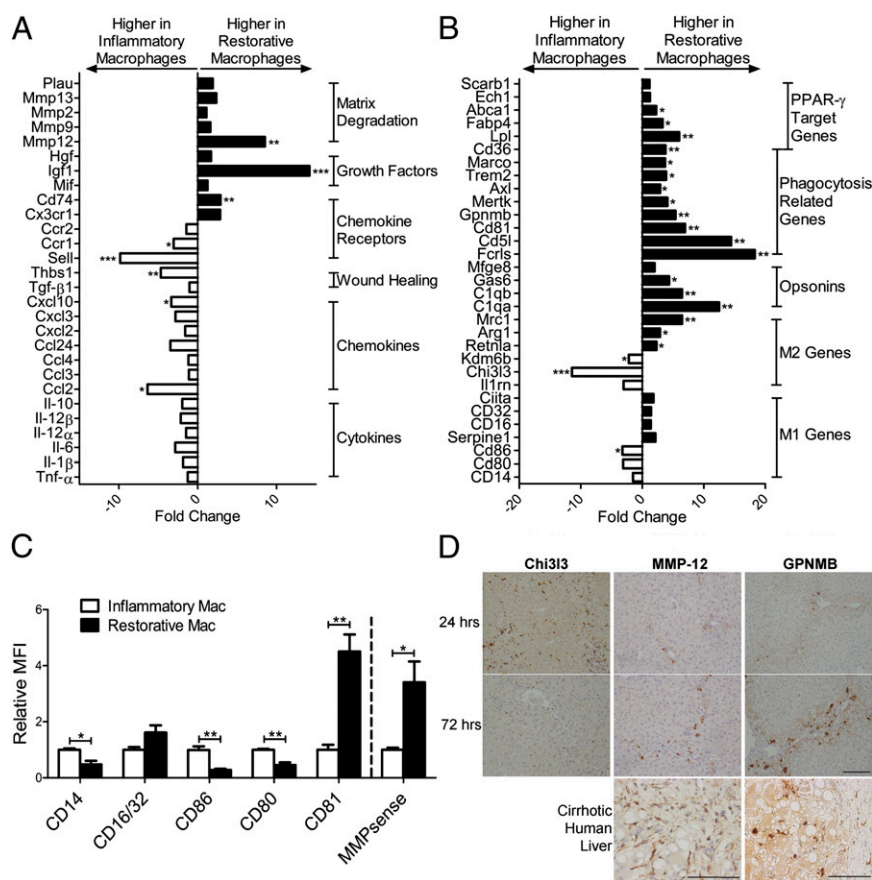


Fig. 5. Ly-6C^{lo} macrophages show a gene expression profile favoring scar resolution. (A and B) Microarray analysis of inflammatory Ly-6C^{hi} and restorative Ly-6C^{lo} hepatic macrophage populations isolated by FACS sorting from livers 24 and 72 h after the final CCl₄ injection, respectively. (A) Differential regulation of cytokines, chemokines, chemokine receptors, growth factors, and matrix-degrading enzymes between the inflammatory and restorative macrophage populations (expressed as fold change between the two macrophage subsets). (B) Differential expression of opsonins, phagocytosis-related genes, PPAR-γ target genes, and macrophage phenotype markers (M1, classical; M2, alternative) between the macrophage subsets on microarray (expressed as fold change between the two macrophage populations). All microarray data based on *n* = 3 per group taken from two independent experiments. **P* < 0.05, ***P* < 0.01, ****P* < 0.001. (C) Flow cytometric analysis comparing expression of stated marker between inflammatory Ly-6C^{hi} and restorative Ly-6C^{lo} hepatic macrophages. MMPsense was administered 24 h before the time of harvest to compare MMP activity between macrophage subsets expressed relative to average MFI for inflammatory macrophage subset (*n* = 3–6). MFI, mean fluorescence intensity. **P* < 0.05, ***P* < 0.01. (D) Immunohistochemistry for genes differentially regulated on microarray in murine liver at 24 and 72 h time points and cirrhotic human liver (representative images shown). (Scale bars: 100 μm).

These data indicate that the phenotypic switch to the restorative macrophage population results in a loss of proinflammatory gene expression, increased expression of matrix-degrading enzymes, and enrichment of phagocytosis-related genes. Furthermore, the identified macrophage phenotypes fall outside the M1/M2 paradigm, highlighting the limitations of this classification in an *in vivo* setting.

Restorative Ly-6C^{lo} Macrophages Are Postphagocytic. Having identified up-regulation of phagocytosis-related pathways, we determined if restorative macrophages were postphagocytic. It is recognized that ingestion of cellular debris can influence macrophage phenotype (42). Furthermore, the switch to fibrosis resolution in our model followed a reduction in hepatocyte death as assessed by serum ALT and AST (Fig. 1D), indicating that the increase in the restorative Ly-6C^{lo} population (Fig. 2E and F) occurred after the clearance of cellular debris.

Flow cytometric and immunohistochemical analysis showed that, compared with the proinflammatory 24-h Ly-6C^{hi} macrophages, restorative 72-h Ly-6C^{lo} macrophages were larger [forward scatter area (FSC-A)], were more complex [side scatter area (SSC-A)], and showed features of being postingestion (Fig. 6A and B). We FACS sorted these two macrophage subsets and TUNEL stained each to quantify the presence of intra- or extracellular apoptotic debris using confocal microscopy (Fig. 6C). No difference was seen in the percentage of each macrophage subset associated with TUNEL-positive debris (Fig. 6D). However, in the proinflammatory macrophages, apoptotic debris was predominantly bound to the cell surface, whereas in the restorative macrophage subset, the debris had been ingested (Fig. 6C and E), confirming the postphagocytic phenotype of the Ly-6C^{lo} macrophage population. These findings are consistent with the known ability of monocytes to bind apoptotic debris, but a

delayed capacity to ingest until differentiation into a more mature macrophage subtype has occurred (43, 44).

Macrophage Phagocytosis *In Vitro* Induces a Matrix-Degrading Phenotype Through ERK Signaling. Having identified evidence of prior phagocytosis as a key feature of the restorative macrophage population, we sought to model this phenotype *in vitro*. Given that the predominant cellular debris in the CCl₄ model is hepatocyte-derived, we determined whether ingestion of hepatocyte debris might induce a similar change in macrophage phenotype. Primary bone marrow-derived macrophages (BMDMs), widely used to study macrophage biology *in vitro* (45), were cultured in the presence and absence of cell debris generated from strain-matched primary murine hepatocytes. Macrophage morphology changed significantly after coculture in keeping with ingestion of hepatocyte debris (Fig. 7A). Hepatocyte debris alone did not attach to the wells. After ingestion, BMDMs up-regulated *Mmp12*, *Mmp9*, and *Igf1* and down-regulated *Thbs1* and *Chi3l3* (Fig. 7B), mirroring the phenotypic switch seen *in vivo* (Fig. 5A and B). To confirm the active secretion of MMPs and determine if this effect was a general effect of phagocytosis on macrophages independent of the type of debris, we used the well-described model of phagocytosis of apoptotic thymocytes (46). Culture supernatants from BMDMs fed with apoptotic thymocytes for 12 h showed a robust increase in active MMP-9 and MMP-12 secretion detected by gelatin zymography and Western blotting, respectively (Fig. 7C and D).

We then sought to determine which signaling pathways might link macrophage phagocytosis with the increase in matrix-degrading activity. MAPK signaling, specifically the ERK and p38 cascades, is activated in macrophages after phagocytosis, and it has been reported to regulate a number of macrophage responses (47, 48). Using immunohistochemistry, we could identify nuclear phos-

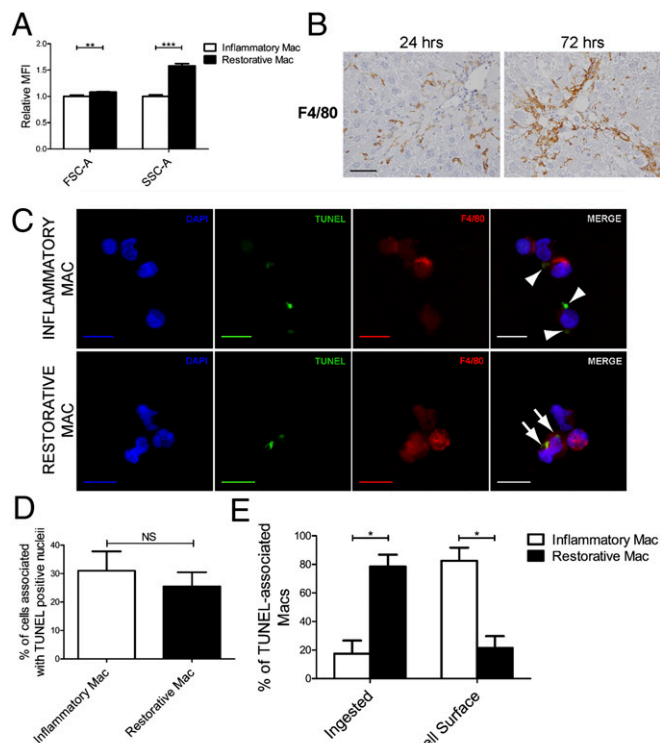


Fig. 6. Restorative Ly-6C^{lo} macrophages are postphagocytic. Comparison of inflammatory (24 h Ly-6C^{hi}) and restorative (72 h Ly-6C^{lo}) macrophage subsets after 4 wk of CCl₄. (A) Size [forward scatter area (FSC-A)] and complexity [side scatter area (SSC-A)] of macrophage subsets assessed by flow cytometry expressed relative to average MFI for inflammatory macrophages (*n* = 13 from three independent experiments). (B) F4/80 immunohistochemistry shows larger scar-associated macrophages at 72 h. (Scale bar: 50 μm.) (C–E) TUNEL staining and confocal microscopy of FACS-sorted subsets. (C) Stained DAPI, TUNEL, F4/80, and merged image for macrophage subsets. (Scale bars: 10 μm.) Arrowheads, cell-surface debris; arrows, ingested debris. (D) Percentage of each subset associated with TUNEL-positive nuclei by cell counting (*n* = 3–4). (E) Percentage of TUNEL-associated macrophages with ingested or cell-surface debris (*n* = 3–4). Data shown as mean ± SEM. **P* < 0.05, ***P* < 0.01, ****P* < 0.001. NS, nonsignificant. Representative images are shown.

pho-ERK staining in macrophages at the 72-h time point (Fig. 7E), indicating activation of the ERK signaling pathway in scar-associated macrophages during maximal fibrosis resolution. To show a functional role for ERK signaling in the observed macrophage phenotype, we administered the specific ERK kinase [mitogen-activated protein kinase kinase 1 and 2 (MEK1/2)] inhibitor PD98059 (50 μM) or vehicle control to BMDMs at published doses (49, 50) for 1 h before and during feeding with hepatocyte debris in vitro. Administration of PD98059 significantly inhibited macrophage up-regulation of Mmp9, Mmp12, and Igf1 in response to the ingestion of hepatocyte debris (Fig. 7F). Furthermore, casein zymography on culture supernatants showed that ERK inhibition abrogated the increase in active MMP-9 and MMP-12 secretion observed after phagocytosis (Fig. 7G), indicating a critical role for MEK1/2 activation in the increased matrix-degrading activity in macrophages in response to phagocytosis. MEK1/2 inhibition had no effect on the down-regulation of Thbs1 and Chi3l3 in response to phagocytosis (Fig. S7A), suggesting that cross-talk between signaling pathways is required for generating the complex overall phenotype of the restorative macrophage. We confirmed the role of MEK1/2 in macrophage Mmp12 up-regulation in response to phagocytosis using a second specific inhibitor UO126 (20 μM) (Fig. S7B). Administration of a p38 MAPK inhibitor (SB203580; 10 μM) at a published dose (51) had no effect

on macrophage expression of Mmp9, Mmp12, or Igf1 in response to phagocytosis (Fig. S7C).

These data show that the matrix-degrading phenotype of the proresolution macrophage can be modeled in vitro by the phagocytosis of cellular debris, and this phenotypic switch is, at least in part, mediated by phagocytosis-related MEK1/2 activation and ERK signaling in macrophages.

Induction of Phagocytic Behavior Using Liposomes Enhances the Restorative Macrophage Phenotype in Vivo and Accelerates Fibrosis Resolution. Having conclusively identified macrophage phagocytosis as a key determinant of the proresolution matrix-degrading phenotype, we wished to use this information to manipulate

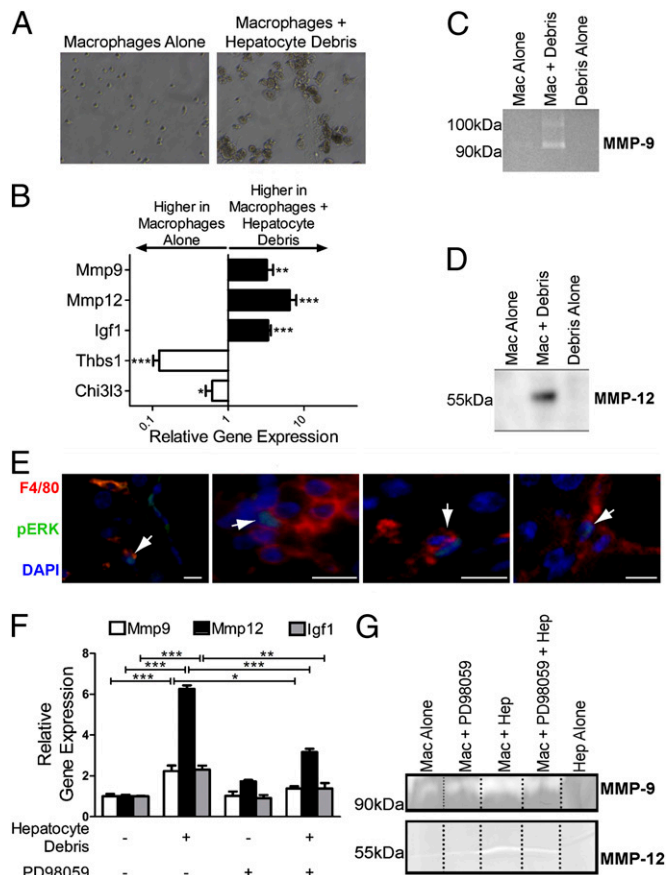


Fig. 7. Macrophage phagocytosis in vitro induces a matrix-degrading phenotype through ERK signaling. (A and B) Coculture of BMDMs with hepatocyte debris. (A) Changes in macrophage morphology on phase-contrast microscopy. Hepatocyte debris alone was nonadherent. (B) Changes in macrophage gene expression after coculture expressed relative to mean expression of macrophages alone (*n* = 11–12 from two independent experiments). (C and D) Coculture of BMDMs with apoptotic thymocytes. (C) Gelatin zymography of culture supernatants equalized for protein content showing active MMP-9 (representative zymogram from *n* = 4 from two independent experiments). (D) Western blot for MMP-12 on culture supernatants equalized for protein content (representative blot from *n* = 4 from two independent experiments). (E) Dual immunofluorescence for F4/80 and phospho-ERK in mouse liver 72 h after final CCl₄ dose after 4 wk of injury. Arrows, nuclear pERK and F4/80 dual positive cells. (Scale bars: 10 μm.) (F and G). Culture of BMDMs ± MEK1/2 inhibitor (PD98059; 50 μM) ± hepatocyte debris. (F) Changes in macrophage gene expression after coculture expressed relative to mean expression of macrophages alone (*n* = 6). (G) Casein zymography of culture supernatants equalized for protein content showing active MMP-9 and MMP-12 (representative zymogram from *n* = 3 shown). Data shown as mean ± SEM. **P* < 0.05, ***P* < 0.01, ****P* < 0.001. Representative images are shown.

macrophage phenotype *in vivo* with a therapeutic benefit in accelerating fibrosis resolution. The systemic administration of cellular debris is likely to have significant confounding off-target effects. Liposome uptake by macrophages represents a genuine phagocytosis event (52), and it has been widely used to target macrophages *in vivo*. Furthermore, recent studies have shown that liposome administration can alter macrophage phenotype *in vivo* in part by induction of ERK signaling after ingestion (53, 54). We proceeded to feed BMDMs with liposomes *in vitro*, which induced a change in macrophage phenotype (Fig. 8A) analogous to the change that we observed *in vivo* (Fig. 5A and B) and similar to the tissue culture models after the ingestion of cellular debris (Fig. 7B). Thus, ingestion of liposomes models the phagocytosis of cellular debris and the generation of restorative macrophages. We went on to administer liposomes (or vehicle control) to chronically injured mice during maximal fibrosis resolution for 48, 72, and 96 h after the final CCl₄ injection, with harvest at 120 h (Fig. 8B). In keeping with an induction of phagocytic behavior, liposome administration caused a reduction in proinflammatory Ly-6C^{hi} macrophages and an increase in restorative Ly-6C^{lo} hepatic macrophages during fibrosis resolution (Fig. 8C). Liposomes, when fluorescently labeled, were rarely detected in Ly-6C^{hi} macrophages but frequently seen in Ly-6C^{lo} macrophages, indicative of a postphagocytic phenotype (Fig. 8D). Critically, this manipulation accelerated the regression of liver fibrosis (Fig. 8E and F), indicating that, by inducing phagocytosis, macrophages could be switched to a phenotype promoting fibrosis resolution *in vivo*.

Discussion

In a murine model of reversible hepatic fibrosis, we have used differential Ly-6C expression to identify and characterize the hitherto elusive restorative macrophage. This Ly-6C^{lo} CD11B^{hi} F4/80^{int} macrophage population accumulates in the liver, and it is the main MMP-expressing macrophage subset during maximal fibrosis resolution, is necessary for degradation of tissue scar, is derived from infiltrating Ly-6C^{hi} inflammatory monocytes, has a distinct pattern of gene expression, including matrix degradation and phagocytic and growth factors, and is characterized by evidence of prior phagocytosis of dying cells. The restorative phenotype can be recapitulated *in vitro* by phagocytosis-induced ERK signaling and can be induced *in vivo* by the administration of liposomes, which accelerates scar resolution.

Although evidence for a central role for macrophages in inflammation and tissue fibrogenesis has been described across organ systems (8), data have recently emerged to suggest a functional heterogeneity of subtypes *in vivo* and a role in fibrosis resolution (3, 6, 11, 12). Differential Ly-6C expression has been widely used to identify functionally distinct populations of circulating murine monocytes (15, 16) and macrophage populations in pathology (17–21). Our data show that Ly-6C expression can be exploited to identify the macrophage subset responsible for fibrosis resolution. Key questions arising from studies regarding the divergent role of macrophages in fibrogenesis and recovery were whether these distinct functions were mediated by resident or recruited cells and whether those cells underwent a phenotypic switch *in situ* (55, 56). Herein, we have shown conclusively that the proresolution Ly-6C^{lo} macrophage population derives from recruited Ly-6C^{hi} monocytes, a common origin to the profibrotic Ly-6C^{hi} macrophage, indicating a switch in macrophage function *in vivo*. This finding is in keeping with the known ability of monocytes and macrophages to change phenotype *in situ* depending on local environmental cues (13). These findings have implications for development of antifibrotic therapies, where targeting inflammatory monocyte recruitment might adversely impact on the population of restorative Ly-6C^{lo} macrophages (39, 57). This finding provides an explanation for the apparently counterintuitive observation made in the work by Mitchell et al. (58): that decreased CCR2-dependent recruitment of Ly-6C^{hi}

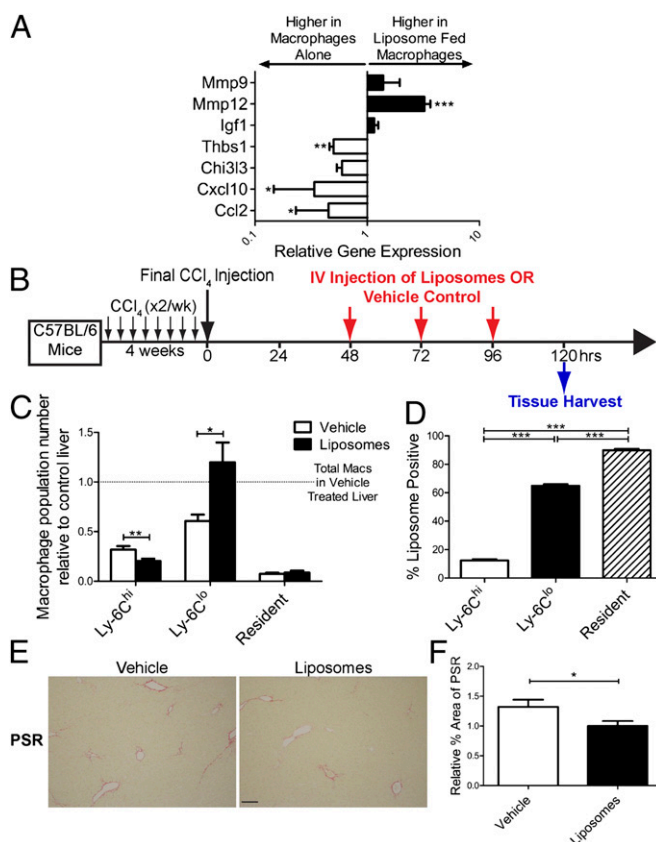


Fig. 8. Induction of phagocytic behavior using liposomes enhances the restorative macrophage phenotype *in vivo* and accelerates fibrosis resolution. (A) Changes in macrophage gene expression after *in vitro* feeding with liposomes expressed relative to mean expression of unfed macrophages ($n = 6$). (B) Schematic representation of the model of liposome (or vehicle) administration during resolution phase after 4 wk of CCl₄ injury. (C) Changes in hepatic macrophage subsets after liposome administration relative to mean total macrophage number in vehicle-treated livers ($n = 13$ –14). (D) Percentage of each hepatic macrophage subset containing fluorescently labeled liposomes assessed by flow cytometry ($n = 8$). (E) Fibrosis assessed by PSR staining after liposome (or vehicle) administration. Representative images are shown. (Scale bar: 100 μ m.) (F) Quantification of fibrosis by morphometric pixel analysis expressed relative to mean percent area for liposome-treated liver ($n = 6$). Data shown as mean \pm SEM. * $P < 0.05$, ** $P < 0.01$, *** $P < 0.001$.

monocytes retards fibrosis resolution (58). A more detailed study of the signals controlling macrophage dynamics and phenotype during fibrosis resolution now depends on the development of monocyte/macrophage-specific chemokine receptor KO transgenic mice, in which key genes can be inducibly deleted without the confounding variable of differences in peak fibrosis that complicates noninducible transgenic models.

The contribution of local macrophage proliferation during hepatic fibrogenesis or fibrosis resolution has not previously been defined. We have shown a high level of proliferation of proinflammatory hepatic Ly-6C^{hi} monocyte-derived macrophages, suggesting that a combination of recruitment and local proliferation is required for the generation of restorative Ly-6C^{lo} macrophages. This finding initially seems to contrast with findings in work by Jenkins et al. (31), where resident F4/80^{hi} pleural macrophages proliferated during chronic parasitic infection. However, using classical inflammatory stimuli, the work by Jenkins et al. (31) also showed the capacity of recruited monocyte-derived macrophages to proliferate in the context of IL-4 stimulation (31). Our work is, therefore, complementary to this study, highlighting that the relative contribution of recruitment and

local proliferation to tissue macrophage expansion during inflammation is critically dependent on the nature of injury and organ involved. Investigators should consider this information in future studies on macrophage dynamics.

A major difficulty in studying macrophage heterogeneity in vivo is the lack of defined specific markers for functionally distinct populations, necessitating the use of flow cytometry on freshly isolated tissue to recognize subsets. Thus, existing strategies for macrophage depletion are unable to specifically select for functionally distinct subsets. In this work, we used the widely used CD11B-DTR system (11, 17). This transgenic strategy shows selectivity for CD11B^{hi} F4/80^{lo} monocytes and monocyte-derived macrophages compared with CD11B^{lo} F4/80^{hi} resident tissue macrophages. We have gone on to show that specific depletion of subsets of CD11B^{hi} F4/80^{lo} cells is critically dependent on timing. Furthermore, our data indicate an increased susceptibility of Ly-6C^{lo} macrophages to depletion with DT, which is likely to be a result of higher levels of CD11B expression in this population. We have discovered a number of genes that are differentially expressed by the functionally distinct populations. These findings could inform transgenic studies, where individual macrophage subsets could be specifically depleted or labeled in vivo. Using these data, we could identify distinct macrophages in situ using immunohistochemistry, enabling more easy translation to studying human tissue. Our findings are based on the highly tractable and predictable CCl₄ model of reversible hepatic fibrosis. To study macrophage dynamics and phenotype on a day-by-day basis, we deliberately focused on an early fibrosis, which resolves rapidly and completely. A future goal is the more detailed analysis of hepatic macrophage subsets in cirrhotic human liver to identify analogous populations to those populations described in this study; until this analysis is undertaken, extrapolation of our findings to human models must be guarded.

The data presented also show that the switch to a proresolution macrophage population confers a number of potential antifibrotic properties. Principally, there is a change from expression of proinflammatory cytokines, chemokines, and profibrotic genes, such as thrombospondin-1 (34), to a profile incorporating genes responsible for scar degradation, such as Mmp12 and Mmp9, genes critical for the clearance of cellular debris, and a number of potential antifibrotic pathways, such as Igf1 (35) and CD74/MIF (33). Furthermore, our data expose the limitations of categorizing macrophage populations from an in vivo setting into the widely used but restrictive M1/M2 paradigm. Moving forward, we suggest that a more functional classification of macrophage subsets should be used to better represent their biology.

Phagocytosis can elicit significant effects on macrophage phenotype and function (19, 42). By showing that the proresolution macrophage phenotype can be promoted by ingestion of debris and that the increase in matrix-degrading activity is mediated by phagocytosis-induced ERK signaling, we have identified a potential therapeutic approach to manipulate these cells in situ. Crucially, our data showing that the in vivo phenotypic switch can be induced through phagocytosis of administered liposomes with a beneficial effect on fibrosis resolution identify a possible translational strategy for the treatment of tissue fibrosis. An attractive alternative therapeutic strategy would be the use of macrophages modified in vitro by feeding with liposomes to generate proresolution features as a cell therapy to induce fibrosis regression. This use would require modification of the macrophages to ensure adequate trafficking to the fibrotic liver after peripheral injection, but it remains an intriguing area for additional study.

In conclusion, we have identified and characterized a specific macrophage phenotype responsible for the resolution of tissue fibrosis. In addition to the value in studying macrophage biology, this study has important implications for fibrosis research and the future development of antifibrotic therapies aimed at targeting macrophages in vivo.

Materials and Methods

Mice. C57BL/6 mice (CD45.2⁺) were purchased from Harlan. CD11B-DTR mice, originally obtained from R. Lang, Children's Hospital Research Foundation, Cincinnati, OH and as previously described (11), were maintained as heterozygotes on a C57BL/6 background. CD45.1⁺ C57BL/6 mice (59) were provided by S. M. Anderton, University of Edinburgh. CD11C-DOG mice (28) were provided by A. S. MacDonald, University of Edinburgh. Mice were bred under specific pathogen-free conditions at the University of Edinburgh. All experiments had local ethical approval and were conducted under UK Home Office Legislation.

Liver Fibrosis Models. Adult male mice at least 6 wk of age were used. Hepatic fibrosis was induced by two times per week i.p. CCl₄ (0.4 μ L/g; Sigma) diluted 1:3 in olive oil (Sigma) for 4 wk (nine injections). Animals were culled at stated time points after the final CCl₄ injection. For depletion studies, DT (10 ng/g in PBS; List Biological Laboratories) or PBS control was administered to fibrotic CD11B-DTR or WT mice i.v. through the tail vein at the stated time points. DC depletion in fibrotic CD11C-DOG mice was performed by administration of DT (12 ng/g) or PBS control i.p. at the stated time points. Adoptive transfer experiments were performed through the tail vein at stated time points using (i) 9×10^5 FACS-sorted CD45.1⁺ Ly-6C^{hi} monocytes from bone marrow in RPMI 1640 or vehicle control; (ii) 250 μ L fluorescent latex beads [0.5 μ m Fluoresbrite polychromatic red microspheres; 2.5% solids (wt/vol) diluted 1:25 in PBS for injection; Polysciences Inc] or vehicle control; and (iii) 250 μ L liposomes (60) (provided by N.v.R.), CM-Dil-labeled (Invitrogen) liposomes (labeled according to the manufacturer's protocol), or PBS control.

Flow Cytometry and FACS Sorting. Flow cytometry (using BD LSR Fortessa II) and FACS sorting (using BD FACSaria II) were performed on hepatic nonparenchymal cells containing the total hepatic leukocyte population (*SI Materials and Methods*). FACS sorting routinely yielded cell purity levels of over 95%.

Detection of in Vivo MMP Activity. To detect in vivo MMP activity, 2 nmol MMPsense 680 (Perkin-Elmer) (or vehicle control) were administered to animals through the tail vein 24 h before harvest according to the manufacturer's protocol. Hepatic macrophages were identified using flow cytometry followed by identification of MMPsense-positive macrophages with excitation laser at 635 nm (23).

Microarray Analysis. Fifty nanograms RNA from FACS-sorted cells was processed using the Ovation Pico WTA system (NuGen) according to the manufacturer's protocol ($n = 3$ per group). Processed RNAs were hybridized to Affymetrix GeneChip Mouse Gene 1.0 ST Arrays. RNA/microarray processing was carried out by ARK Genomics (Roslin Institute). Data analysis was performed as described (*SI Materials and Methods*). Fold change > 2 with adjusted $P < 0.05$ was considered significant for individual gene changes. Gene ontology and Kyoto Encyclopedia of Genes and Genomes (KEGG) pathway enrichment analysis was done with the DAVID tool (36, 37) on genes that were significantly differentially expressed. Microarray data are available in the ArrayExpress database (www.ebi.ac.uk/arrayexpress) under accession number E-MEXP-3177.

In Vitro Phagocytosis Assay. BMDMs, primary murine hepatocyte debris, and apoptotic thymocytes were prepared as described (*SI Materials and Methods*); 2×10^5 BMDMs were seeded per well in 12-well plates followed by the addition of 5×10^5 washed dead hepatocytes (or control medium) and 1×10^6 washed dead thymocytes or liposomes at 1:10 dilution by volume (or PBS control) cultured for 16 h (or 12 h for thymocytes) at 37 °C 5% (vol/vol) CO₂ in DMEM/F12 Glutamax (Gibco) medium with 10% FCS. Where stated, inhibitors PD98059 (50 μ M; Cayman Chemical), UO126 (20 μ M; New England Biolabs), SB203580 (10 μ M; Cayman Chemical), or DMSO control were added to the plated BMDMs for 1 h before and maintained throughout the 16-h incubation with hepatocyte debris. Supernatants were then harvested and stored at -80 °C, noningested hepatocytes or liposomes were removed by vigorous washing three times with PBS, and residual adherent macrophages were used for additional analysis. In control wells containing hepatocyte debris alone, no adherent cells were detected.

Statistical Analysis. All data are expressed as mean \pm SEM. Statistical analysis was performed using GraphPad Prism 5 software. Statistical evaluation of multiple groups was performed using a one-way ANOVA with posthoc Tukey test. Statistical evaluation of two groups was performed using Student t test or Mann-Whitney test if data were not normally distributed. A value of $P < 0.05$ was considered statistically significant.

Additional Methods. Additional methods are shown in *SI Materials and Methods*.

ACKNOWLEDGMENTS. We thank Prof. S. M. Anderton for providing the CD45.1 mice and Dr. A. S. MacDonald for providing CD11c-DOG mice. P.R., M.A.V., and V.K.S. were supported by Wellcome Trust Research Training Fellowships. A.P., R.L.A., S.N.H., and J.P.I. were supported by a Medical

Research Council Programme grant. L.B. was supported by a Medical Research Council PhD studentship. A.A. was supported by the Royal College of Surgeons of Edinburgh. T.T.G.-W. and M.J.W. were supported by Medical Research Council Research Training Fellowships. D.R.D. and J.R.M. were supported in part by the Edinburgh British Heart Foundation Centre of Research Excellence. J.A.F. was supported by the Academy of Medical Sciences and the Health Foundation. S.J.F. was supported by the Sir Jules Thorn Trust.

- Hayden T (2011) Scarred by disease. *Nat Med* 17(1):18–20.
- Wynn TA (2008) Cellular and molecular mechanisms of fibrosis. *J Pathol* 214(2):199–210.
- Ramachandran P, Iredale JP (2009) Reversibility of liver fibrosis. *Ann Hepatol* 8(4):283–291.
- Eddy AA (2005) Can renal fibrosis be reversed? *Pediatr Nephrol* 20(10):1369–1375.
- Pickrell JA, Diel JH, Slauson DO, Halliwell WH, Mauderly JL (1983) Radiation-induced pulmonary fibrosis resolves spontaneously if dense scars are not formed. *Exp Mol Pathol* 38(1):22–32.
- Gibbons MA, et al. (2011) Ly6Chi monocytes direct alternatively activated profibrotic macrophage regulation of lung fibrosis. *Am J Respir Crit Care Med* 184(5):569–581.
- Tyralla K, et al. (2011) High-dose enalapril treatment reverses myocardial fibrosis in experimental uremic cardiomyopathy. *PLoS One* 6(1):e15287.
- Wynn TA, Barron L (2010) Macrophages: Master regulators of inflammation and fibrosis. *Semin Liver Dis* 30(3):245–257.
- Vernon MA, Mylonas KJ, Hughes J (2010) Macrophages and renal fibrosis. *Semin Nephrol* 30(3):302–317.
- Hardie WD, Glasser SW, Hagood JS (2009) Emerging concepts in the pathogenesis of lung fibrosis. *Am J Pathol* 175(1):3–16.
- Duffield JS, et al. (2005) Selective depletion of macrophages reveals distinct, opposing roles during liver injury and repair. *J Clin Invest* 115(1):56–65.
- Fallowfield JA, et al. (2007) Scar-associated macrophages are a major source of hepatic matrix metalloproteinase-13 and facilitate the resolution of murine hepatic fibrosis. *J Immunol* 178(8):5288–5295.
- Mosser DM, Edwards JP (2008) Exploring the full spectrum of macrophage activation. *Nat Rev Immunol* 8(12):958–969.
- Mantovani A, et al. (2004) The chemokine system in diverse forms of macrophage activation and polarization. *Trends Immunol* 25(12):677–686.
- Gordon S, Taylor PR (2005) Monocyte and macrophage heterogeneity. *Nat Rev Immunol* 5(12):953–964.
- Ingersoll MA, et al. (2010) Comparison of gene expression profiles between human and mouse monocyte subsets. *Blood* 115(3):e10–e19.
- Lin SL, Castaño AP, Nowlin BT, Lupher ML, Jr., Duffield JS (2009) Bone marrow Ly6Chigh monocytes are selectively recruited to injured kidney and differentiate into functionally distinct populations. *J Immunol* 183(10):6733–6743.
- Nahrendorf M, et al. (2007) The healing myocardium sequentially mobilizes two monocyte subsets with divergent and complementary functions. *J Exp Med* 204(12):3037–3047.
- Arnold L, et al. (2007) Inflammatory monocytes recruited after skeletal muscle injury switch into antiinflammatory macrophages to support myogenesis. *J Exp Med* 204(5):1057–1069.
- Movahedi K, et al. (2010) Different tumor microenvironments contain functionally distinct subsets of macrophages derived from Ly6C(high) monocytes. *Cancer Res* 70(14):5728–5739.
- Karlmarm KR, et al. (2009) Hepatic recruitment of the inflammatory Gr1+ monocyte subset upon liver injury promotes hepatic fibrosis. *Hepatology* 50(1):261–274.
- Holt MP, Cheng L, Ju C (2008) Identification and characterization of infiltrating macrophages in acetaminophen-induced liver injury. *J Leukoc Biol* 84(6):1410–1421.
- Cortez-Retamozo V, et al. (2008) Real-time assessment of inflammation and treatment response in a mouse model of allergic airway inflammation. *J Clin Invest* 118(12):4058–4066.
- Sunderkötter C, et al. (2004) Subpopulations of mouse blood monocytes differ in maturation stage and inflammatory response. *J Immunol* 172(7):4410–4417.
- Bamboat ZM, et al. (2010) Conventional DCs reduce liver ischemia/reperfusion injury in mice via IL-10 secretion. *J Clin Invest* 120(2):559–569.
- Jiao J, et al. (2012) Dendritic cell regulation of carbon tetrachloride-induced murine liver fibrosis regression. *Hepatology* 55(1):244–255.
- Hume DA (2008) Macrophages as APC and the dendritic cell myth. *J Immunol* 181(9):5829–5835.
- Phytian-Adams AT, et al. (2010) CD11c depletion severely disrupts Th2 induction and development in vivo. *J Exp Med* 207(10):2089–2096.
- Tacke F, et al. (2006) Immature monocytes acquire antigens from other cells in the bone marrow and present them to T cells after maturing in the periphery. *J Exp Med* 203(3):583–597.
- Tacke F, et al. (2007) Monocyte subsets differentially employ CCR2, CCR5, and CX3CR1 to accumulate within atherosclerotic plaques. *J Clin Invest* 117(1):185–194.
- Jenkins SJ, et al. (2011) Local macrophage proliferation, rather than recruitment from the blood, is a signature of Th2 inflammation. *Science* 332(6035):1284–1288.
- Karlmarm KR, et al. (2010) The fractalkine receptor CX3CR1 protects against liver fibrosis by controlling differentiation and survival of infiltrating hepatic monocytes. *Hepatology* 52(5):1769–1782.
- Heinrichs D, et al. (2011) Macrophage migration inhibitory factor (MIF) exerts antifibrotic effects in experimental liver fibrosis via CD74. *Proc Natl Acad Sci USA* 108(42):17444–17449.
- Breitkopf K, et al. (2005) Thrombospondin 1 acts as a strong promoter of transforming growth factor beta effects via two distinct mechanisms in hepatic stellate cells. *Gut* 54(5):673–681.
- Sobrevals L, et al. (2010) Insulin-like growth factor I gene transfer to cirrhotic liver induces fibrolysis and reduces fibrogenesis leading to cirrhosis reversion in rats. *Hepatology* 51(3):912–921.
- Dennis G, Jr., et al. (2003) DAVID: Database for Annotation, Visualization, and Integrated Discovery. *Genome Biol* 4(5):3.
- Huang W, Sherman BT, Lempicki RA (2009) Systematic and integrative analysis of large gene lists using DAVID bioinformatics resources. *Nat Protoc* 4(1):44–57.
- Anstee QM, Wright M, Goldin R, Thurst MR (2009) Parenchymal extinction: Coagulation and hepatic fibrogenesis. *Clin Liver Dis* 13(1):117–126.
- Sahin H, Trautwein C, Wasmuth HE (2010) Functional role of chemokines in liver disease models. *Nat Rev Gastroenterol Hepatol* 7(12):682–690.
- Lawrence T, Natoli G (2011) Transcriptional regulation of macrophage polarization: Enabling diversity with identity. *Nat Rev Immunol* 11(11):750–761.
- Martinez FO, Gordon S, Locati M, Mantovani A (2006) Transcriptional profiling of the human monocyte-to-macrophage differentiation and polarization: New molecules and patterns of gene expression. *J Immunol* 177(10):7303–7311.
- Savill J, Dransfield I, Gregory C, Haslett C (2002) A blast from the past: Clearance of apoptotic cells regulates immune responses. *Nat Rev Immunol* 2(12):965–975.
- Henson PM, Bratton DL, Fadok VA (2001) Apoptotic cell removal. *Curr Biol* 11(19):R795–R805.
- Newman SL, Henson JE, Henson PM (1982) Phagocytosis of senescent neutrophils by human monocyte-derived macrophages and rabbit inflammatory macrophages. *J Exp Med* 156(2):430–442.
- Marim FM, Silveira TN, Lima DS, Jr., Zamboni DS (2010) A method for generation of bone marrow-derived macrophages from cryopreserved mouse bone marrow cells. *PLoS One* 5(12):e15263.
- Ferenbach DA, et al. (2010) Macrophages expressing heme oxygenase-1 improve renal function in ischemia/reperfusion injury. *Mol Ther* 18(9):1706–1713.
- Kurosaka K, Takahashi M, Kobayashi Y (2003) Activation of extracellular signal-regulated kinase 1/2 is involved in production of CXC-chemokine by macrophages during phagocytosis of late apoptotic cells. *Biochem Biophys Res Commun* 306(4):1070–1074.
- Chung EY, et al. (2007) Interleukin-10 expression in macrophages during phagocytosis of apoptotic cells is mediated by homeodomain proteins Pbx1 and Prep-1. *Immunity* 27(6):952–964.
- Raza SL, Nehring LC, Shapiro SD, Cornelius LA (2000) Proteinase-activated receptor-1 regulation of macrophage elastase (MMP-12) secretion by serine proteinases. *J Biol Chem* 275(52):41243–41250.
- Valledor AF, Comalada M, Xaus J, Celada A (2000) The differential time-course of extracellular-regulated kinase activity correlates with the macrophage response toward proliferation or activation. *J Biol Chem* 275(10):7403–7409.
- Chi H, et al. (2006) Dynamic regulation of pro- and anti-inflammatory cytokines by MAPK phosphatase 1 (MKP-1) in innate immune responses. *Proc Natl Acad Sci USA* 103(7):2274–2279.
- Perry DG, Martin WJ, 2nd (1995) Fluorescent liposomes as quantitative markers of phagocytosis by alveolar macrophages. *J Immunol Methods* 181(2):269–285.
- Ma HM, Wu Z, Nakanishi H (2011) Phosphatidylserine-containing liposomes suppress inflammatory bone loss by ameliorating the cytokine imbalance provoked by infiltrated macrophages. *Lab Invest* 91(6):921–931.
- Harel-Adar T, et al. (2011) Modulation of cardiac macrophages by phosphatidylserine-presenting liposomes improves infarct repair. *Proc Natl Acad Sci USA* 108(5):1827–1832.
- Friedman SL (2005) Mac the knife? Macrophages—the double-edged sword of hepatic fibrosis. *J Clin Invest* 115(1):29–32.
- Wynn TA (2011) Integrating mechanisms of pulmonary fibrosis. *J Exp Med* 208(7):1339–1350.
- Vielhauer V, Kulkarni O, Reichel CA, Anders HJ (2010) Targeting the recruitment of monocytes and macrophages in renal disease. *Semin Nephrol* 30(3):318–333.
- Mitchell C, et al. (2009) Dual role of CCR2 in the constitution and the resolution of liver fibrosis in mice. *Am J Pathol* 174(5):1766–1775.
- O'Connor RA, Leech MD, Suffner J, Hämmerling GJ, Anderton SM (2010) Myelin-reactive, TGF- β -induced regulatory T cells can be programmed to develop Th1-like effector function but remain less proinflammatory than myelin-reactive Th1 effectors and can suppress pathogenic T cell clonal expansion in vivo. *J Immunol* 185(12):7235–7243.
- Van Rooijen N, Sanders A (1994) Liposome mediated depletion of macrophages: Mechanism of action, preparation of liposomes and applications. *J Immunol Methods* 174(1–2):83–93.